Luminescence from Color Centers in $KMgF_3$ †

C. R. Riley*
Solid State Division, Oak Ridge National Laboratory, Oak Ridge, Tennessee 37830

and

S. I. Yun and W. A. Sibley
Physics Department, Oklahoma State University, Stillwater, Oklahoma 74074
(Received 5 November 1971)

A study of the emission from electron- and γ-irradiated $KMgF_3$ crystals reveals bands at 407, 465, 590, 600, and 750 nm. By means of polarized bleaching experiments the bands at 465 and 590 nm can be assigned as due to F_3 and F_2 centers, respectively. In addition, the temperature dependence of both the widths and peak positions of the emission bands can be used to predict approximate values for the absorption energy of the defects responsible for these bands. The predicted absorption is very close to that observed for F_2 and F_3 centers. This lends further confidence to the assignments. The 600-nm emission is believed to be due to Mn^{2+} impurity ions.

I. INTRODUCTION

Recently there have been several investigations of radiation-induced defects in $KMgF_3$ crystals.[1-4] These experiments have dealt primarily with the identification of the optical-absorption bands arising from these defects and with the kinetics of the defects themselves. Very little work has been done on the emission from the various defect centers. We felt that it would be highly desirable to study the emission from irradiated $KMgF_3$ and make assignments of the observed bands to defects induced by radiation or present as impurity.

$KMgF_3$ has the cubic perovskite structure and in this structure the F center has a D_{4h} symmetry, $F_2(M)$ centers have C_{2v} symmetry, and $F_3(R)$ centers have C_{3v} symmetry. Optical bleaching with the appropriate wavelength of $[1\bar{1}0]$ and/or $[100]$ polarized light has been shown to result in anisotropic absorption characteristic of $\langle 110\rangle$ oriented centers (F_2) at 282 and 445 nm and $\langle 111\rangle$ oriented centers (F_3) at 250 and 395 nm.[3] Once the defects have been rearranged into orientations which are no longer random it should be possible to observe polarized luminescence from these defects, and to use this polarized emission to identify the defects responsible for the various emission bands seen after irradiation. Thus, the purpose of this paper is to determine the luminescence bands due to F_2 and F_3 centers and to measure the temperature dependence of the half-width and peak positions of these bands.

II. EXPERIMENTAL PROCEDURE

The crystals were grown by the Stockbarger method in an argon atmosphere using purified starting material. A graphite crucible was used and the growth rate was 3 mm/h.[5] An impurity analysis of these crystals has been published previously.[3]

Specimens about 1 mm thick were cut from the crystal ingots and polished. Irradiations were performed either with ^{60}Co γ rays or 2.0-MeV electrons. When low-temperature measurements were desired a Sulfrian liquid-helium cryostat was used and the required temperature was maintained either with an electrical heater system or by using the appropriate liquified gases or freons. The temperature of the samples was monitored during irradiation and optical measurements by means of a platinum resistance thermometer mounted in the sample holder.

Optical-absorption measurements were made

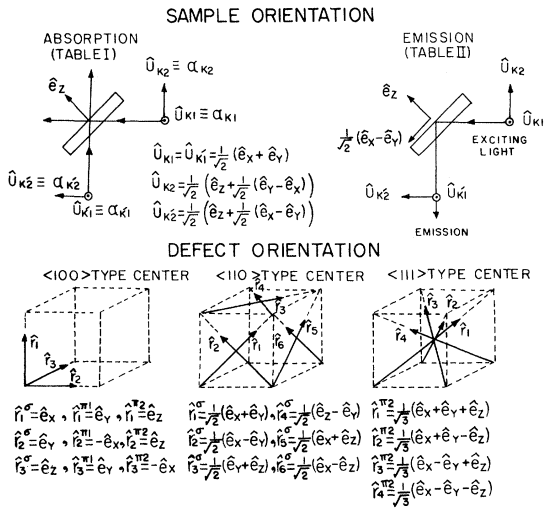

FIG. 1. Schematic illustrations of the sample orientation with respect to both the incident light and the detection systems for absorption and emission and of defect orientations in cubic crystals.

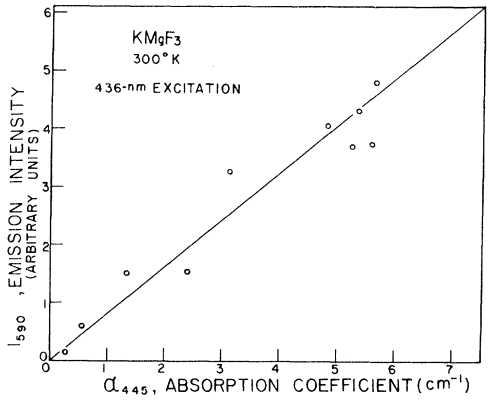

FIG. 2. Plot of the emission intensity at 590 nm due to 436-nm light excitation vs the absorption coefficient at 445 nm.

using a Cary-14 or Cary-15 spectrophotometer with matched Polaroid HNP'B uv polarizers. Polarized bleaching was accomplished with a mercury lamp, appropriate filter, and a polarizer. The luminescence detection system consisted of an EMI-9558 or an RCA-7102 photomultiplier tube, cooled to dry-ice temperature to reduce dark current, mounted to a 1-m Jarrell-Ash monochromator. The detection system was calibrated using a standard quartz-iodine lamp with calibration traceable to the Bureau of Standards. In the case of luminescence measurements the calibration for polarized emission is difficult since the monochromator has a preferential polarization and the exciting light in some cases must be reflected from a mirror which also gives preferential polarization. We feel the calibration for polarized light is reliable to about 10%. The sample is placed at about a 45° angle from both the exciting light direction and detection direction and is slightly off-angle to minimize reflection of the exciting light into the detection system. A diagram of the sample orientation with respect to the excitation and detection systems is shown in Fig. 1.

III. THEORY

Although the theoretical calculations for polarized absorption and emission by oriented defects have been published in the past[6] in the interest of clarity and especially since sample orientation plays a major role in the calculations, we will briefly review these calculations as they apply to our experimental situation. Figure 1 is a schematic of the sample orientation, with respect to both the exciting light and the detection system, and of the orientation of different types of defects in a cubic lattice. The major electric dipole axis is designated σ, the dipole axis perpendicular to σ but in the same {100} plane is shown as π_1, and the dipole axis perpendicular to both of these directions is labeled π_2. The unit vectors $\hat{e}_x$, $\hat{e}_y$, and $\hat{e}_z$ are the [100], [010], and [001] directions, respectively. For the case of absorption when the incident light is polarized along a direction $\hat{\eta}$ the interaction of this light with the various defect configurations $\hat{r}_i^{\beta}$, where β is either the major electric dipole axis σ or one of the minor electric dipole axes π_1 or π_2, results in an absorption coefficient given by the expression

$$\alpha_{\hat{\eta}} = \bar{\sigma}\sum_i n_i |\hat{\eta}\cdot\hat{r}_i^{\sigma}|^2 + \bar{\pi}_1\sum_i n_i |\hat{\eta}\cdot\hat{r}_i\pi_1|^2 + \bar{\pi}_2\sum_i n_i |\hat{\eta}\cdot\hat{r}_i\pi_2|^2 . \quad (1)$$

Here $\bar{\sigma}$, $\bar{\pi}_1$, and $\bar{\pi}_2$ are factors unique to the dipole axes and contain several constants,[5] and n_i is the number of centers whose major axis σ lies along one of the orientations shown in Fig. 1. The results of this type of calculation are shown in Table I for light propagating along the $\hat{U}_{K2}$, $\hat{U}_{K'2}$, and [001] directions. The notation α_{K2} denotes the

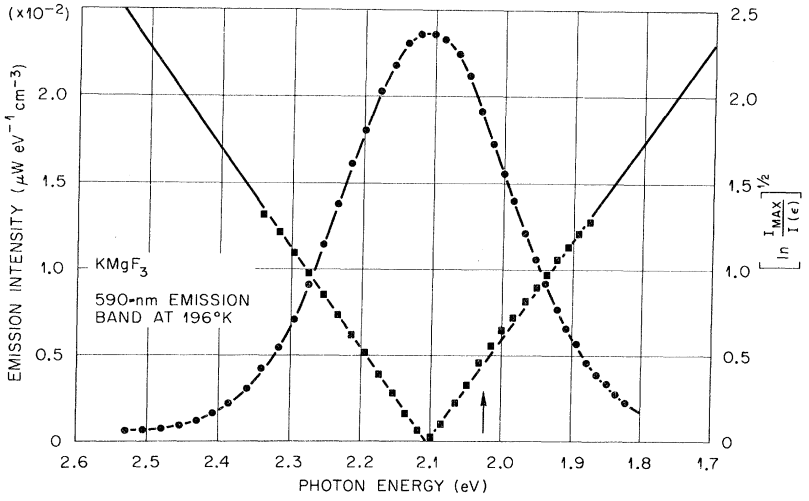

FIG. 3. 590-nm emission band at 196°K.

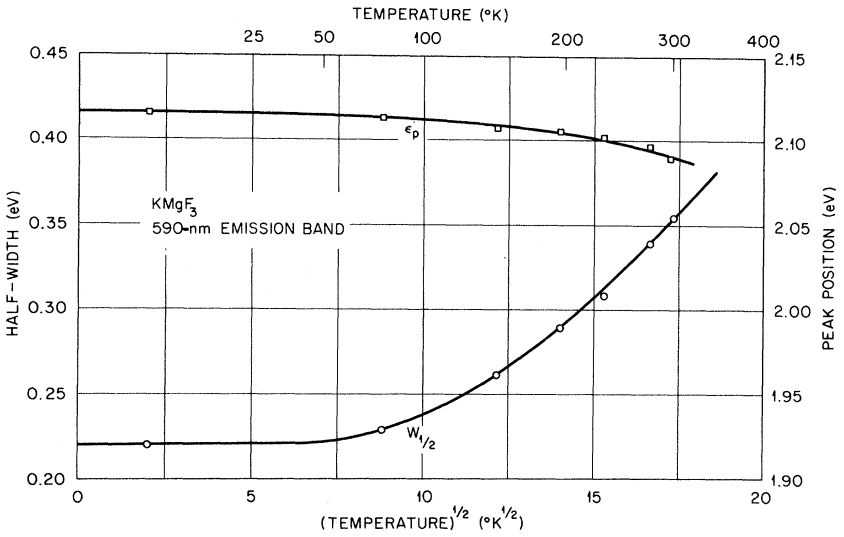

FIG. 4. Temperature dependence of half-width and peak position of the 590-nm emission band.

absorption coefficient for light polarized along the $\hat{U}_{K2}$ direction. The square of the direction cosine between light propagating in the $\hat{U}_{K'2}$ direction and polarized along the direction $\hat{U}_{K2}$ and $\hat{r}_3^\beta$ and $\hat{r}_6^\beta$ is denoted as $\frac{1}{8}\delta$; and $\frac{1}{8}\gamma$ is the square of the direction cosine between $\hat{U}_{K2}$ and $\hat{r}_4^\beta$ and $\hat{r}_5^\beta$. For the sample orientation used in this experiment, i.e., 45° to the incident beam, $\delta=(\sqrt{2}+1)^2$ and $\gamma=(\sqrt{2}-1)^2$. When the light is perpendicular to the sample face, the equation is much simplified

TABLE I. Absorption coefficient for linearly polarized light as a function of the type of center.

Absorption coefficient	⟨110⟩-type center	⟨111⟩-type center
$\alpha_{K1}(\epsilon)=\alpha_{K'1}(\epsilon)$	$\sigma(\epsilon)[n_1+\frac{1}{4}(n_3+n_4+n_5+n_6)]$ $+\pi_1(\epsilon)[n_2+\frac{1}{4}(n_3+n_4+n_5+n_6)]$ $+\pi_2(\epsilon)[\frac{1}{2}(n_3+n_4+n_5+n_6)]$	$\sigma(\epsilon)[\frac{1}{6}(n_1+n_2)+\frac{1}{2}(n_3+n_4)]$ $+\pi_1(\epsilon)[\frac{1}{6}(n_1+n_2)+\frac{1}{2}(n_3+n_4)]$ $+\frac{2}{3}\pi_2(\epsilon)(n_1+n_2)$
$\alpha_{K2}(\epsilon)$	$\sigma(\epsilon)[\frac{1}{2}n_2+\frac{1}{8}\delta(n_3+n_6)+\frac{1}{8}\gamma(n_4+n_5)]$ $+\pi_1(\epsilon)[\frac{1}{2}n_1+\frac{1}{8}\gamma(n_3+n_6)+\frac{1}{8}\delta(n_4+n_5)]$ $+\pi_2(\epsilon)[\frac{1}{2}(n_1+n_2)+\frac{1}{4}(n_3+n_4+n_5+n_6)]$	$\frac{1}{12}\sigma(\epsilon)(5n_1+5n_2+\delta n_3+\gamma n_4)$ $+\frac{1}{12}\pi_1(\epsilon)(5n_1+5n_2+\delta n_3+\gamma n_4)$ $+\frac{1}{6}\pi_2(\epsilon)(n_1+n_2+\gamma n_3+\delta n_4)$
$\alpha_{K'2}(\epsilon)$	$\sigma(\epsilon)[\frac{1}{2}n_2+\frac{1}{8}\gamma(n_3+n_6)+\frac{1}{8}\delta(n_4+n_5)]$ $+\pi_1(\epsilon)[\frac{1}{2}n_1+\frac{1}{8}\delta(n_3+n_6)+\frac{1}{8}\gamma(n_4+n_5)]$ $+\pi_2(\epsilon)[\frac{1}{2}(n_1+n_2)+\frac{1}{4}(n_3+n_4+n_5+n_6)]$	$\frac{1}{12}\sigma(\epsilon)(5n_1+5n_2+\gamma n_3+\delta n_4)$ $+\frac{1}{12}\pi_1(\epsilon)(5n_1+5n_2+\gamma n_3+\delta n_4)$ $+\frac{1}{6}\pi_2(\epsilon)(n_1+n_2+\delta n_3+\gamma n_4)$
$\alpha_{1\bar{1}0}(\epsilon)$	$\sigma(\epsilon)[n_1+\frac{1}{4}(n_3+n_4+n_5+n_6)]$ $+\pi_1(\epsilon)[n_2+\frac{1}{4}(n_3+n_4+n_5+n_6)]$ $+\frac{1}{2}\pi_2(\epsilon)[n_3+n_4+n_5+n_6]$	$\frac{1}{6}\sigma(\epsilon)(n_1+n_2+3n_3+3n_4)$ $+\frac{1}{6}\pi_1(\epsilon)(n_1+n_2+3n_3+3n_4)$ $+\frac{2}{3}\pi_2(\epsilon)(n_1+n_2)$
$\alpha_{1\bar{1}0}(\epsilon)$	$\sigma(\epsilon)[n_2+\frac{1}{4}(n_3+n_4+n_5+n_6)]$ $+\pi_1(\epsilon)[n_1+\frac{1}{4}(n_3+n_4+n_5+n_6)]$ $+\frac{1}{2}\pi_2(\epsilon)[n_3+n_4+n_5+n_6]$	$\frac{1}{6}\sigma(\epsilon)(3n_1+3n_2+n_3+n_4)$ $+\frac{1}{6}\pi_1(\epsilon)(3n_1+3n_2+n_3+n_4)$ $+\frac{2}{3}\pi_2(\epsilon)(n_3+n_4)$

TABLE II. Relative intensities for polarized emission.

Type of Center	α β	I_{11}	I_{12}	I_{21}	I_{22}
<100>	σ-σ	$\frac{1}{4}\rho[n_1 + n_2]$ $\frac{1}{2}\rho\bar{n}$	$\frac{1}{8}\rho[n_1 + n_2]$ $\frac{1}{4}\rho\bar{n}$	$\frac{1}{8}\rho[n_1 + n_2]$ $\frac{1}{4}\rho\bar{n}$	$\frac{1}{16}\rho[n_1 + n_2 + 4n_3]$ $\frac{3}{8}\rho\bar{n}$
	σ-π	$\frac{1}{8}\rho[n_1 + n_2]$ $\frac{1}{4}\rho\bar{n}$	$\frac{3}{16}\rho[n_1 + n_2]$ $\frac{3}{8}\rho\bar{n}$	$\frac{1}{16}\rho[n_1 + n_2 + 4n_2]$ $\frac{3}{8}\rho\bar{n}$	$\frac{1}{32}\rho[3n_1 + 3n_2 + 4n_3]$ $\frac{5}{16}\rho\bar{n}$
	π-σ	$\frac{1}{8}\rho[n_1 + n_2]$ $\frac{1}{4}\rho\bar{n}$	$\frac{1}{16}\rho[n_1 + n_2 + 4n_2]$ $\frac{3}{8}\rho\bar{n}$	$\frac{3}{16}\rho[n_1 + n_2]$ $\frac{3}{8}\rho\bar{n}$	$\frac{1}{32}\rho[3n_1 + 3n_2 + 4n_3]$ $\frac{5}{16}\rho\bar{n}$
	π-π	$\frac{1}{16}\rho[n_1 + n_2 + 4n_3]$ $\frac{3}{8}\rho\bar{n}$	$\frac{1}{32}\rho[3n_1 + 3n_2 + 4n_3]$ $\frac{5}{16}\rho\bar{n}$	$\frac{1}{32}\rho[3n_1 + 3n_2 + 4n_3]$ $\frac{5}{16}\rho\bar{n}$	$\frac{1}{64}\rho[9n_1 + 9n_2 + 4n_3]$ $\frac{11}{32}\rho\bar{n}$
<110>	σ-σ	$\frac{1}{16}\rho[16n_1 + n_3 + n_4 + n_5 + n_6]$ $\frac{5}{4}\rho\bar{n}$	$\frac{1}{32}\rho[\gamma(n_3 + n_6) + \delta(n_4 + n_5)]$ $\frac{3}{8}\rho\bar{n}$	$\frac{1}{32}\rho[\delta(n_3 + n_6) + \gamma(n_4 + n_5)]$ $\frac{3}{8}\rho\bar{n}$	$\frac{1}{64}\rho[16n_2 + n_3 + n_4 + n_5 + n_6]$ $\frac{5}{16}\rho\bar{n}$
	$\sigma-\pi_1$	$\frac{1}{16}\rho[n_3 + n_4 + n_5 + n_6]$ $\frac{1}{4}\rho\bar{n}$	$\frac{1}{32}\rho[16n_1 + \delta(n_3 + n_6) + \gamma(n_4 + n_5)]$ $\frac{7}{8}\rho\bar{n}$	$\frac{1}{32}\rho[16n_2 + \delta(n_3 + n_6) + \gamma(n_4 + n_5)]$ $\frac{7}{8}\rho\bar{n}$	$\frac{1}{64}\rho[\delta^2(n_3 + n_6) + \gamma^2(n_4 + n_5)]$ $\frac{17}{16}\rho\bar{n}$
	$\sigma-\pi_2$	$\frac{1}{8}\rho[n_3 + n_4 + n_5 + n_6]$ $\frac{1}{2}\rho\bar{n}$	$\frac{1}{16}\rho[8n_1 + n_3 + n_4 + n_5 + n_6]$ $\frac{3}{4}\rho\bar{n}$	$\frac{1}{16}\rho[\delta(n_3 + n_6) + \delta(n_4 + n_5)]$ $\frac{3}{4}\rho\bar{n}$	$\frac{1}{32}\rho[8n_2 + \delta(n_3 + n_6) + \gamma(n_4 + n_5)$ $\frac{5}{8}\rho\bar{n}$
<111>	σ-σ π_1-σ σ-π_1 π_1-π_1	$\frac{1}{36}\rho[n_1 + n_2 + 9n_3 + 9n_4]$ $\frac{5}{9}\rho\bar{n}$	$\frac{1}{72}\rho[5n_1 + 5n_2 + 3\gamma n_3 + 3\delta n_4]$ $\frac{7}{18}\rho\bar{n}$	$\frac{1}{72}\rho[5n_1 + 5n_2 + 3\delta n_3 + 3\gamma n_4]$ $\frac{7}{18}\rho\bar{n}$	$\frac{1}{144}\rho[25n_1 + 25n_2 + n_3 + n_4]$ $\frac{13}{36}\rho\bar{n}$
	σ-π_2 π_1-π_2	$\frac{1}{9}\rho[n_1 + n_2]$ $\frac{2}{9}\rho\bar{n}$	$\frac{1}{36}\rho[n_1 + n_2 + 3\delta n_3 + 3\gamma n_4]$ $\frac{5}{9}\rho\bar{n}$	$\frac{5}{18}\rho[n_1 + n_2]$ $\frac{5}{9}\rho\bar{n}$	$\frac{1}{72}\rho[5n_1 + 5n_2 + \delta^2 n_3 + \gamma^2 n_4]$ $\frac{11}{18}\rho\bar{n}$
	π_2-σ π_2-π_1	$\frac{1}{9}\rho[n_1 + n_2]$ $\frac{2}{9}\rho\bar{n}$	$\frac{1}{18}\rho[5n_1 + 5n_2]$ $\frac{5}{9}\rho\bar{n}$	$\frac{1}{36}\rho[n_1 + n_2 + 3\gamma n_3 + 3\delta n_4]$ $\frac{5}{9}\rho\bar{n}$	$\frac{1}{72}\rho[5n_1 + 5n_2 + \gamma^2 n_3 + \delta^2 n_4]$ $\frac{11}{18}\rho\bar{n}$
	π_2-π_2	$\frac{4}{9}\rho[n_1 + n_2]$ $\frac{8}{9}\rho\bar{n}$	$\frac{1}{9}\rho[n_1 + n_2]$ $\frac{2}{9}\rho\bar{n}$	$\frac{1}{9}\rho[n_1 + n_2]$ $\frac{2}{9}\rho\bar{n}$	$\frac{1}{36}\rho[n_1 + n_2 + n_3 + n_4]$ $\frac{1}{9}\rho\bar{n}$

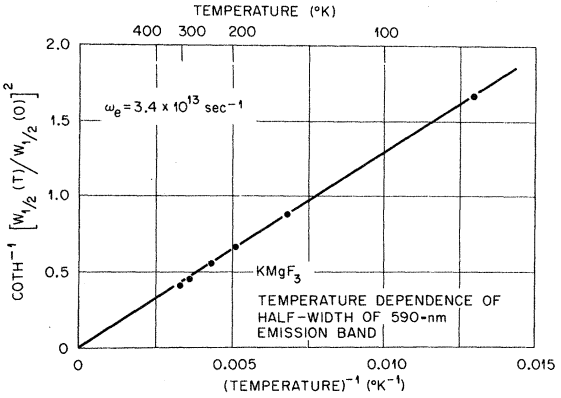

FIG. 5. Temperature dependence of half-width of the 590-nm emission band.

as can be seen from the expression for α_{110}.

Now we will compare the relative intensities of the polarized emission from ⟨110⟩- and ⟨111⟩-type centers. The emission may be written in the form

$$I_{jl} = \rho \sum_i n_i \left| \hat{r}_i^{\beta_1} \cdot \hat{u}_{K'j} \right|^2 \left| \hat{r}_i^{\beta_2} \cdot \hat{u}_{Kl} \right|^2 , \qquad (2)$$

where ρ is a constant and j and l denote the polarization of the excitation and emission respectively, e.g., $j, l = 1, 2$ and $\hat{U}_{Kl}$ and $\hat{U}_{K'j}$ are the polarization vectors shown in Fig. 1 for emission. Note that the emission is not required to be from the same state involved in absorption and the cases $\beta_1, \beta_2 = \sigma$, π_1; π_2 have also been considered. The computed intensities are shown in Table II. The second row in each case gives the value for a random distribution of centers. The absorption coefficients for the directions connected with these measurements are also given in Table I. When both polarized emission and absorption data are available an intercomparison of the two sets of data allows a determination of the defect population

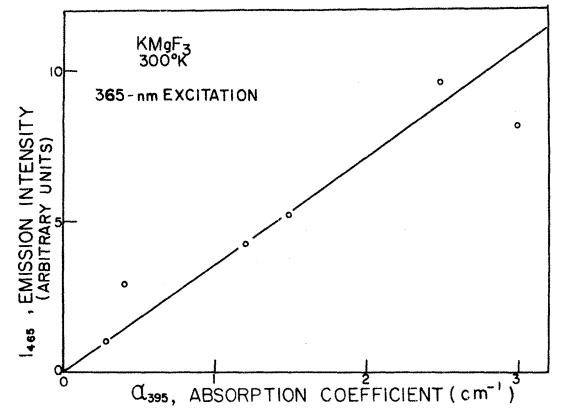

FIG. 6. Emission intensity at 465 nm due to 365-nm light excitation as a function of the absorption coefficient at 395 nm.

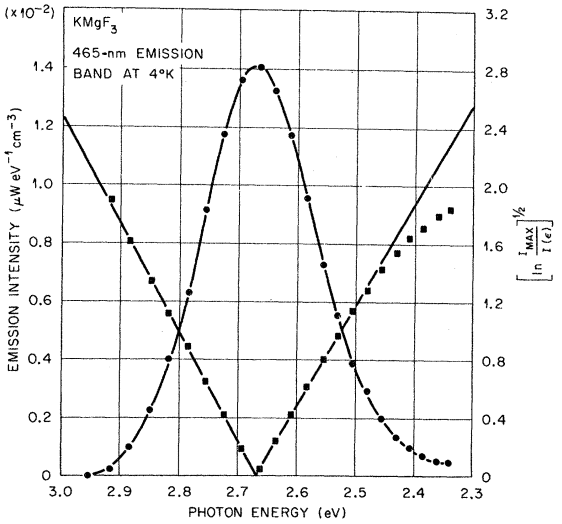

FIG. 7. Gaussian plot of the 465-nm emission band for a sample temperature of 4 °K.

for the various orientations shown in Fig. 1.

IV. RESULTS

When a sample of $KMgF_3$ is irradiated with 2.0-MeV electrons or ^{60}Co γ rays and is then excited with light of wavelengths 254, 313, 365, 436, 405, or 577 nm various emission bands are observed. We will first consider the emission due to F_2 centers which is excited by 436-nm light and occurs at 590 nm, then the emission due to F_3 centers which can be excited with 405-nm light and occurs at 465 nm, and last the emission bands which occur at 407 and 600 nm.

A. F_2(590 nm) Emission

In order to show that the 590-nm emission band is connected with F_2 centers two experiments were

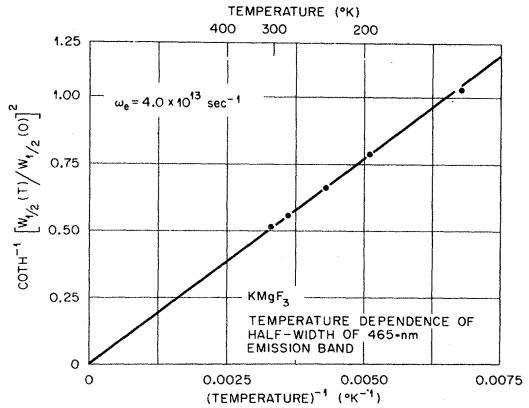

FIG. 8. Temperature dependence of half-width of 465-nm emission band.

TABLE III. Emission intensity ratios for samples bleached with polarized light and the defect distributions determined from the ratios.

Emission intensity ratios (590 nm)	Polarization of bleaching light [1$\bar{1}$0]	[100]	[110]	random
I_{12}/I_{11}	0.252	0.186	0.12	0.30
I_{21}/I_{22}	0.673	1.06	1.20	1.20
I_{22}/I_{11}	0.427	0.22	0.122	0.25
Defect distributions			$\bar{n}=\frac{1}{6}\sum_{i=1}^{6} n_i$	
n_1	$0.94\bar{n}$	$1.36\bar{n}$	$1.98\bar{n}$	$\bar{n}$
n_2	$1.75\bar{n}$	$1.15\bar{n}$	$0.87\bar{n}$	$\bar{n}$
n_3+n_6	$1.77\bar{n}$	$1.93\bar{n}$	$1.75\bar{n}$	$2\bar{n}$
n_4+n_5	$1.54\bar{n}$	$1.55\bar{n}$	$1.40\bar{n}$	$2\bar{n}$

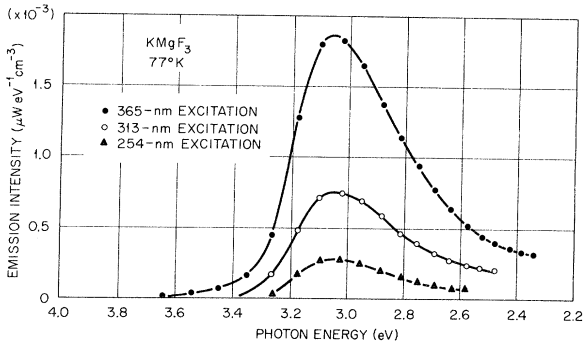

FIG. 9. Emission at 407 nm for a $KMgF_3$ sample at 77 °K.

performed. First, the emission intensity of the band was measured as a function of the absorption coefficient at the peak of the F_2 optical-absorption band (445 nm). The results are illustrated in Fig. 2 and the straight-line relationship suggests that the 590-nm band is due to F_2 centers. The second study dealt with orienting F_2 centers with polarized 254-nm light and then observing the emission to find the band or bands that were polarized. In Table III, the observed polarized luminescence values are analyzed by the relations for the σ-σ case in Table II and the defect distributions, present after polarized bleaching, are determined. Using these values and the relations $\pi_1 = 0.29\sigma$ and $\pi_2 = 0.48\sigma$ which are obtained from the polarized absorption, the agreement between the emission and absorption measurements can be evaluated as shown in Table IV and appears to be very good. Thus, the experimental results again suggest that the 590-nm band is due to F_2 centers.

A study of the variation with temperature of the half-width, $W_{1/2}$, of the 590-nm band was also performed. A Gaussian plot for the 590-nm band at 196 °K is portrayed in Fig. 3. There is some uncertainty as to the accuracy of the low-energy side of the band because of other emission bands and absolute calibration problems. The band is assumed to be symmetric and the energy difference between the high-energy side and the peak is used as a measure of the half-width. This procedure will give a slightly different value for $W_{1/2}$ since the band is probably not a true Gaussian. The variation with temperature of the half-width and the peak position ϵ_{max} for the 590-nm band is shown in Fig. 4. Figure 5 shows a plot of $\coth^{-1}[W_{1/2}(T)/W_{1/2}(0)]^2$ vs $1/T$. A value of the frequency of the dominant interacting phonon mode of $\omega_e = 3.4\times10^{13}\ \mathrm{sec}^{-1}$ is obtained from the slope of the line in Fig. 5 and the expression[7,8]

$$W_{1/2}(T) = W_{1/2}(0)[\coth(\hbar\omega_e/2kT)]^{1/2} \quad . \qquad (3)$$

B. F_3(465 nm) Emission

Studies similar to those described above for F_2 centers were carried out for F_3 center absorption and emission. Figure 6 indicates a definite relationship between the emission band at 465 nm and the absorption band due to F_3 centers (395 nm). Moreover, after the F_3 centers are oriented by a polarized optical bleach the emission at 465 nm is

TABLE IV. Observed and predicted absorption coefficients from oriented F_2 centers.

	[1$\bar{1}$0] bleach		[110] bleach	
Abs. coeff.	Predicted abs. from luminescence	Obs. abs. coeff.	Predicted abs. from luminescence	Obs. abs. coeff.
α_{110}	$3.30\sigma\bar{n}$	5.2	$4.01\sigma\bar{n}$	5.9
$\alpha_{1\bar{1}0}$	$3.88\sigma\bar{n}$	7.0	$3.21\sigma\bar{n}$	4.3
α_{K2}	$3.71\sigma\bar{n}$	6.4	$3.40\sigma\bar{n}$	3.9
α_{K2}'	$3.59\sigma\bar{n}$	6.1	$3.22\sigma\bar{n}$	3.8
$\alpha_{110}/\alpha_{1\bar{1}0}$	0.87	0.74	1.25	1.37
α_{K2}/α_{K2}'	1.03	1.05	1.05	1.03

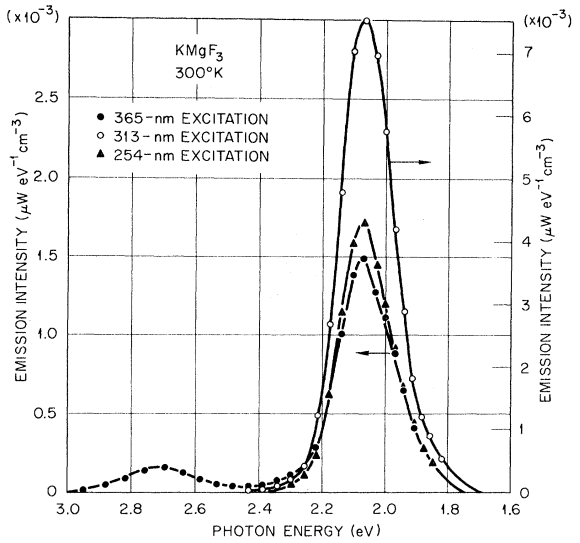

FIG. 10. Emission at 600 nm due to several excitation energies for a sample at 300 °K.

also polarized. These results suggest that the 465-nm emission is due to F_3 centers.

A study of the temperature variation of the half-width of the 465-nm band was made in addition to the above experiments. Figure 7 shows a Gaussian plot for this band for data taken at 4 °K. The tail seen on the low-energy side of the emission results from a small 590-nm emission band which is also excited by a 405-nm excitation. The variation with temperature of $W_{1/2}$ is given in Fig. 8 where a plot of $\coth^{-1}[W_{1/2}(T)/W_{1/2}(0)]^2$ vs $1/T$ can be analyzed to yield a dominant phonon mode frequency ω_e of 4.0×10^{13} sec^{-1}.

C. Other Emission Bands

As mentioned earlier, emission bands at 407 and 600 nm are observed in these irradiated crystals. Both of these bands are seen at 77 °K after irradiation with electrons when the crystal is excited with either 254- , 313- , or 365-nm light. The 407-nm emission, which is depicted in Fig. 9, shows a rapid decrease in quantum efficiency above 77 °K and is most easily observed when only F centers are present in the crystal. Thus, it is tempting to attribute this emission to F centers, but much work must yet be done before such an assignment can be made. On the other hand, the 600-nm emission band has all the characteristics of impurity emission. The quantum efficiency of the emission increases with increasing temperature, crystals doped with Mn show a bright orange emission close to 600 nm, and Mn^{2+} emission in MgF_2 occurs at 590 nm. Therefore, we believe that this band is due to the trace amounts of Mn present in our crystals. The 600-nm emission band is shown in Fig. 10 for several different exciting frequencies.

When a crystal is irradiated at low temperatures, warmed to room temperature, and then recooled to 77 °K new emission bands are observed. In particular, since the warming allows F centers to aggregate, the 690- and 465-nm bands described above are observed. In addition, after aggregation occurs excitation with 577-nm light produces an emission band at 750 nm.

V. DISCUSSION AND SUMMARY

In a previous paper[3] it was pointed out that the phonon modes interacting most strongly with the ground state of F and F_2 centers have an average frequency of 3.4×10^{13} sec^{-1}. Our results in this investigation indicate that the same frequencies are active in interacting with the excited states of the F_2 and F_3 centers. This means that, at least within the restrictions of the simple theory where $\omega_e=\omega_g$, we can predict the Stokes shift for the luminescence bands due to F_2 and F_3 centers since we can determine the Huang-Rhys factor from the expression[7,8]

$$S=[W_{1/2}(0)/2.36\hbar\omega]^2 \tag{4}$$

and the energy of the emission ϵ from[7,8]

$$\epsilon=E_{\mathrm{ABS}}-2S\hbar\omega\ , \tag{5}$$

where E_{ABS} is the absorption energy of the defect. From Eqs. (4) and (5) absorption from F_2 centers is predicted to occur at 426 nm (2.91 eV), whereas it actually is at 440 nm (2.81 eV). In the case of the F_3 center the prediction is 367 nm (3.38 eV) and the experimental value is 395 nm (3.14 eV). The Huang-Rhys factors are 13.7 for the F_3 emission and 17.9 for the F_2 emission process. This latter value can be compared with the $S=11$ number determined for F_2 centers in the absorption process. The high S numbers characteristic of these defects indicate that zero-phonon lines will not be observable.[8] This precludes the construction of relatively accurate configuration coordinate diagrams since zero-phonon lines are a necessity for an unambiguous interpretation. However, such diagrams can be constructed from the information given above if desired.[5]

A consideration of Tables III and IV suggests that only light polarized along the π electric-dipole axis of the defects is efficient at reorienting centers. This observation is further verified by attempts at bleaching not in the 270-nm region (where the absorption is due to π transitions) but in the 445-nm band itself. In this case, no reorientation of centers was observed. The distribution of defects shown in Table III for the different polarizations of bleaching light suggests that F_2 centers re-

orient by 60° jumps, e.g., a defect with a [110] $\hat{r}_1$ orientation can only jump to $\hat{r}_3$, $\hat{r}_4$, $\hat{r}_5$, and $\hat{r}_6$ orientations. As mentioned earlier the good agreement between the absorption coefficient ratios predicted from the polarized luminescence measurements and those values actually observed, as given in Table IV, indicates that the emission is due to F_2 centers and that it is primarily a σ-σ transition.

Dreyfus[9] and Schneider[10] have investigated the reorientation of F_A centers and F_2 centers, respectively. Schneider found that F_2 centers reorient indirectly by the formation of F_2^+ centers which then absorb light and rotate. When the reoriented F_2^+ centers capture electrons then reoriented F_2 centers are formed. F_2^+ centers have not yet been observed in $KMgF_3$; however, our data are not inconsistent with this interpretation.

In summary it has been shown that F_2 centers have absorption transitions at 282- and 445-nm and an emission at 590 nm. F_3 centers absorb light of 250 and 396 nm and emit light of 465 nm. Both of these color centers can be reoriented by polarized bleaching light, but the exact mechanism for this reorientation is not yet known.

†This research was supported by the U. S. AEC under contract with Union Carbide Corp., by AEC equipment Grant No. AT-(40-1)-4080, and by the National Science Foundation.

*Present address: Spin-Labs, Knoxville, Tenn.

[1]T. P. P. Hall, Brit. J. Appl. Phys. 17, 1011 (1966).

[2]T. P. P. Hall and A. Leggeat, Solid State Commun. 7, 1651 (1969).

[3]C. R. Riley and W. A. Sibley, Phys. Rev. B 1, 2789 (1970).

[4]T. L. Lewis, J. L. Kolopus, and E. Sonder (unpublished).

[5]C. R. Riley, Ph. D. thesis (University of Tennessee, 1970) (unpublished).

[6]P. P. Feofilov, *The Physical Basis of Polarized Emission* (Consultants Bureau, New York, 1961).

[7]J. J. Markham, in *Solid State Physics*, edited by F. Seitz and D. Turnbull (Academic, New York, 1966), Suppl. 8; Rev. Mod. Phys. 31, 956 (1959).

[8]D. B. Fitchen, in *The Physics of Color Centers*, edited by W. B. Fowler (Academic, New York, 1968).

[9]R. W. Dreyfus, Phys. Rev. B 1, 4826 (1970).

[10]I. Schneider, Phys. Rev. Letters 24, 1296 (1970).

PHYSICAL REVIEW B VOLUME 5, NUMBER 8 15 APRIL 1972

Ultrasonic Propagation, Stress Effects, and Interaction Parameters at the Displacive Transition in $SrTiO_3$

K. Fossheim

Department of Physics, University of Trondheim, Norges Tekniske Høgskole, Trondheim, Norway

and

B. Berre*

Department of Physics, University of Oslo, Oslo, Norway

(Received 16 September 1971)

The interaction between strain and order parameter at the structural transition in $SrTiO_3$ is investigated by ultrasonic measurements of attenuation, velocity shifts, and stress dependence of the transition temperature T_a. A method is described by which measurements of domain attenuation are used to correct the velocity data below T_a. Also, biaxial pressure has been successfully used to suppress the domain structure in the tetragonal phase. By comparing the experimental results with the consequences of a phenomenological configurational potential the interaction parameters are deduced. The model is found to correlate the experimental results in a consistent way. The hydrostatic-pressure dependence of T_a is predicted to be $dT_a/dp = 0.5 \times 10^{-3}$ K/dyn cm^{-2}. Critical effects in sound velocity and attenuation are briefly described.

I. INTRODUCTION

During the past few years the compound $SrTiO_3$ has attracted increasing attention from different branches of solid-state physics. The primary reason for the interest in this material is the fact that its structural transition is associated with a condensation of a (triply degenerate) lattice mode, often referred to as a soft mode. $SrTiO_3$ has, in fact, become a major testing ground for the soft-mode theory of solid-state transitions.[1] Furthermore, $SrTiO_3$ belongs to a family of perovskite-type compounds—including, for instance, $KMnF_3$, $LaAlO_3$, and $CsPbCl_3$—possessing cubic symmetry in the high-temperature phase ($T > T_a$). In the low-temperature phase ($T < T_a$) different symmetries are